PERGAMON

International Journal of Heat and Mass Transfer 44 (2001) 4225–4234

International Journal of HEAT and MASS TRANSFER

www.elsevier.com/locate/ijhmt

Slip-flow heat transfer in rectangular microchannels

Shiping Yu, Timothy A. Ameel *

Department of Mechanical Engineering, University of Utah, 50 S. Central Campus Dr., Rm 2202, Salt Lake City, UT 84112, USA

Received 11 July 2000; received in revised form 16 February 2001

Abstract

Laminar slip-flow forced convection in rectangular microchannels is studied analytically by applying a modified generalized integral transform technique to solve the energy equation, assuming hydrodynamically fully developed flow. Results are given in terms of the fluid mixed mean temperature, and both local and fully developed mean Nusselt numbers. Heat transfer is found to increase, decrease, or remain unchanged, compared to non-slip-flow conditions, depending on two dimensionless variables that include effects of rarefaction and the fluid/wall interaction. The transition point at which the switch from heat transfer enhancement to reduction occurs is identified for different aspect ratios.

1. Introduction

Rarefaction effects must be considered in fluids in which the molecular mean free path is comparable to the system's characteristic length. In this case, the fluid's molecular structure becomes more significant and the continuum assumption is no longer valid. The fluid exhibits non-continuum effects such as slip-flow and thermodynamic non-equilibrium (temperature jump) at the gas–solid interface. Traditional examples of fluids in the slip-flow regime [1] include low-pressure fluids such as those occurring in vacuums and in the upper atmosphere. The recent development of microscale thermal fluid systems has created renewed interest in this field of study. Microfluidic systems typically have characteristic lengths on the order of 1 to 100 μm and are often operated in gaseous environments at standard conditions where the molecular mean free path is on the order of 100 nm. Thus microfluidic systems must take into account rarefaction, or non-continuum, effects even at standard conditions.

The Knudsen number Kn, defined as the ratio of the molecular mean free path λ to the characteristic length of the system, is the parameter used to classify fluids that deviate from continuum behavior. For small values ($Kn \leqslant 10^{-3}$), the fluid is considered to be a continuum, while for large values ($Kn \geqslant 10$), the fluid is considered to be a free molecular flow. The slip-flow regime to be studied here, is near the continuum region and is classified as $10^{-3} < Kn < 10^{-1}$.

Flows in the slip-flow regime have traditionally been modeled using the Navier–Stokes and energy equations modified by boundary conditions that contain the rarefaction effects on the velocity and temperature fields. Eckert and Drake [1] have indicated that there is strong evidence to support this approach. More recently, Liu et al. [2] and Arkilic et al. [3] found that the Navier–Stokes equations, when combined with slip-flow boundary conditions, yield results for pressure drop and friction factor that are in agreement with experimental data for some microchannel flows. The Graetz problem considers the developing temperature field in a circular tube for a fluid that is fully developed hydrodynamically. This traditional problem has been modified through the slip-flow and temperature jump boundary conditions to study internal convective heat transfer occurring in circular tubes in the slip-flow regime. Shih et al. [4], Barron et al. [5,6], and Wang [7] have investigated this problem for an isothermal wall condition. Their results indicate that the rarefaction effects, manifested as slip-flow at the boundary, augment heat transfer. However, there are two simplifications adopted

* Corresponding author. Tel.: +1-801-585-9730; fax: +1-801-585-9826.

E-mail address: ameel@mech.utah.edu (T.A. Ameel).

0017-9310/01/$ - see front matter
PII: S0017-9310(01)00075-8

Nomenclature

a	one-half of channel width
$\hat{a}$	non-dimensional one-half of channel width, a/D
A	defined in Eq. (12)
A_c	cross-sectional area
b	one-half of channel height
$\hat{b}$	non-dimensional one-half of channel height, b/D
B_k	defined in Eq. (13)
D	hydraulic diameter, $4ab/(a+b)$
D_{ijmn}	defined in Eq. (36)
F_k	defined in Eq. (14)
F_t	thermal accommodation coefficient
F_v	tangential momentum accommodation coefficient
G_k	defined in Eq. (15)
h	heat transfer coefficient
k	thermal conductivity
Kn	Knudsen number, λ/D
M	defined in Eq. (33)
N	summation truncation number
N^*	summation truncation number
Nu	local Nusselt number
Nu_∞	fully developed Nusselt number for slip-flow
$Nu_{\infty,ns}$	fully developed Nusselt number for non-slip-flow
Nu_m	mean Nusselt number
p	pressure
P	non-dimensional pressure, $p/(\rho u_m^2)$
Pe	Peclet number, $RePr$
P_{ki}	defined in Eq. (46)
Pr	Prandtl number
Q_{km}	defined in Eq. (45)
R	aspect ratio, b/a
Re	Reynolds number, $u_m D/v$
T	fluid temperature
T_0	inlet fluid temperature
T_w	wall temperature
u	streamwise velocity
u_m	mean streamwise velocity
U	non-dimensional streamwise velocity, u/u_m
x	horizontal transverse coordinate
X	non-dimensional horizontal transverse coordinate, x/D
y	vertical transverse coordinate
Y	non-dimensional vertical transverse coordinate, y/D
z	axial coordinate
Z	non-dimensional axial coordinate, $z/(PeD)$
Greek symbols	
β	non-dimensional variable, β_t/β_v
β_c	transition value of β
β_t	dimensionless variable, defined in Eq. (4)
β_v	dimensionless variable, defined in Eq. (3)
γ	ratio of specific heats
η	eigenvalue, Eq. (29)
v	kinematic viscosity
θ	non-dimensional temperature, $(T-T_w)/(T_0-T_w)$
θ_m	non-dimensional fluid mixed mean temperature
$\bar{\theta}^*_{im}$	transformed potentials
λ	molecular mean free path
μ	dynamic viscosity
ξ	eigenvalue, Eq. (30)
ϕ	eigenvalue, Eq. (16)
Φ_c	defined in Eq. (40)
Φ_{ijk}	defined in Eq. (39)
Φ^*_{mnk}	defined in Eq. (41)
$\Re$	universal gas constant

in these studies that reduce the applicability of the results. First, the temperature jump boundary condition was actually not directly implemented in these solutions. Second, both the thermal accommodation coefficient F_t and the momentum accommodation coefficient F_v were assumed to be unity. This second assumption, while reasonable for most fluid–solid combinations, produces a solution limited to a specific set of fluid–solid conditions. Ameel et al. [8] studied the related Graetz problem involving a constant heat flux at the wall. In this case, increasing rarefaction effects produced a reduction in heat transfer. An indirect solution method, which utilizes the eigenvalue problem for the isothermal case, was implemented. On the other hand, Wang et al. [9] obtained the analytical solution of the extended Graetz problem for isoflux wall conditions through a direct solution method. Once again, the slip effects were shown to reduce heat transfer. In both Ameel et al. [8] and Wang et al. [9], the accommodation coefficients were assumed to have values of unity.

A generalized investigation of the extended Graetz problem was considered by Larrode et al. [10]. The effects of rarefaction and the fluid/wall interaction were included through the introduction of two non-dimensional parameters. One of these dimensionless parameters is a measure of the degree of rarefaction and is the product of the Knudsen number Kn and a term that includes the tangential momentum accommodation coefficient F_v. The second parameter is a function of the surface accommodation coefficients, the ratio of the fluid specific heats γ, and the Prandtl number Pr. The results from Larrode et al. [10] indicate that heat transfer de-

pends both on the degree of rarefaction and on the surface accommodation coefficients. The values of the two non-dimensional parameters were found to influence the heat transfer, which may increase, decrease, or remain unchanged when compared to non-slip-flow. Yu and Ameel [11] studied slip-flow heat transfer in a microscale gap formed from isothermal surfaces. Contrary to all previous studies, axial conduction effects were included. Their results were similar to those of Larrode et al. [10]; however, the inclusion of axial conduction was found to increase heat transfer and the thermal entrance length.

All of the previously mentioned studies were conducted for microtubes with circular cross-sections or, in the case of Yu and Ameel [11], in a microscale gap. However, most microfluidic systems will utilize microchannels with either rectangular or trapezoidal cross-section due to constraints imposed by the most common microfabrication technologies. Papautsky et al. [12] and Stanley et al. [13] describe two technologies, surface micromachining and micromilling, used to create metallic rectangular microchannels for use in micro thermal fluid systems. Thus, in the realization of many proposed microscale thermal fluid systems, rectangular microchannels will be the primary mode of fluid transport. This provides strong motivation for investigations of slip-flow heat transfer in rectangular microchannels.

2. Analysis

Analytical slip-flow studies have traditionally been based on the continuum form of the Navier–Stokes equations and energy equation with the slip-flow effects concentrated in the additional terms in the tangential velocity and temperature boundary conditions [1]. These new boundary conditions represent velocity slip and temperature jump conditions at the gas–surface interface, and for the y-direction are given as [1,14,15]

$$u(x,b) = \left[-\beta_v \lambda \frac{\partial u}{\partial y} + 3\left(\frac{\Re T}{8\pi}\right)^{1/2} \frac{\lambda}{T} \frac{\partial T}{\partial z} \right]_{y=b}, \tag{1}$$

$$T(x,b,z) - T_w = \left[-\beta_t \lambda \frac{\partial T}{\partial y} + \frac{1}{4\Re} u^2 \right]_{y=b}, \tag{2}$$

where β_v and β_t are defined as

$$\beta_v = \frac{2-F_v}{F_v}, \tag{3}$$

$$\beta_t = \frac{2-F_t}{F_t} \frac{2\gamma}{\gamma+1} \frac{1}{Pr} \tag{4}$$

and F_v and F_t are the tangential momentum accommodation coefficient and thermal accommodation coefficient, respectively. F_v and F_t are parameters that describe the gas–surface interaction and are functions of the composition and temperature of the gas, the gas velocity over the surface, and the solid surface temperature, chemical state, and roughness. Values of the accommodation coefficients range from near 0 to 1, where these values represent specular reflection and diffuse reflection, respectively. For most engineering applications, values of the accommodation coefficients are near unity [1,14]; however, F_t may vary in a wide range from 10^{-2} to 1.0 [1]. In non-dimensionalizing the temperature jump boundary conditions, the ratio of β_t to β_v appears and is thus defined as

$$\beta = \frac{\beta_t}{\beta_v}. \tag{5}$$

The first-term in Eq. (1) represents velocity slip due to the y-direction transverse velocity gradient while the second-term represents thermal creep due to the temperature gradient in the flow direction. Since $\lambda \propto T^{-1/2}$, the second-term is second order in λ. At the same time, $\partial/\partial y \gg \partial/\partial z$; thus, the second-term in Eq. (1) is negligible. The first-term in Eq. (2) represents temperature jump due to the y-direction transverse temperature gradient while the second-term represents slip velocity viscous heating [15]. With the typical low Eckert number assumption, this term is also negligible. Therefore, only the first-terms of the two slip-flow boundary conditions will be retained. The slip-flow boundary conditions in the x-direction have a similar form as Eqs. (1) and (2).

The velocity profile for slip-flow can be determined from the z-momentum equation assuming a Newtonian fluid, negligible body forces, constant properties, and fully developed steady state flow. The applicable non-dimensional z-momentum equation is

$$\frac{\partial^2 U}{\partial X^2} + \frac{\partial^2 U}{\partial Y^2} = \frac{1}{Pr} \frac{dP}{dZ}. \tag{6}$$

With the origin of the coordinate system at the centerline of the rectangular channel of sides $2a$ and $2b$ and the x-axis and y-axis in the horizontal and vertical directions, respectively, the flow boundary conditions are

$$\left.\frac{\partial U}{\partial X}\right|_{X=0} = 0, \tag{7}$$

$$\left[U + (\beta_v Kn) \frac{\partial U}{\partial X} \right]_{X=\hat{a}} = 0, \tag{8}$$

$$\left.\frac{\partial U}{\partial Y}\right|_{Y=0} = 0, \tag{9}$$

$$\left[U + (\beta_v Kn)\frac{\partial U}{\partial Y}\right]_{Y=\hat{b}} = 0. \tag{10}$$

Ebert and Sparrow [16] have obtained the non-dimensional velocity profile by solving the problem given by Eqs. (7)–(10). Consistent with Ebert and Sparrow [16], both u and u_m are normalized with $(D^2/\mu)(dp/dz)$; therefore, the pressure gradient is not explicit in U. The solution in terms of the current non-dimensional parameters is

$$U(X,Y) = A\sum_{k=1}^{\infty} B_k F_k(Y) G_k(X), \tag{11}$$

where

$$A = \hat{a}\hat{b}\left\{\sum_{i=1}^{\infty}\phi_i^{-5}\left[\frac{\sin^2(\phi_i\hat{b})}{\hat{b} + (\beta_v Kn)\,\sin^2(\phi_i\hat{b})}\right] \times \left[\phi_i\hat{a} - \frac{\tanh(\phi_i\hat{a})}{1 + (\beta_v Kn)\phi_i \tanh(\phi_i\hat{a})}\right]\right\}^{-1}, \tag{12}$$

$$B_k = \frac{\sin(\phi_k\hat{b})}{\phi_k^3\left[\hat{b} + (\beta_v Kn)\,\sin^2\left(\phi_k\hat{b}\right)\right]}, \tag{13}$$

$$F_k(Y) = \cos(\phi_k Y), \tag{14}$$

$$G_k(X) = 1 - \frac{\cosh(\phi_k X)}{\cosh(\phi_k\hat{a}) + (\beta_v Kn)\phi_k \sinh(\phi_k\hat{a})} \tag{15}$$

and the eigenvalues ϕ_k are determined from the following transcendental equation

$$\cot(\phi_k\hat{b}) = (\beta_v Kn)\phi_k, \quad k = 1,2,3,\ldots \tag{16}$$

For hydrodynamically fully developed flow, high Peclet number, negligible energy dissipation, and constant properties, the dimensionless energy equation and thermal boundary conditions and initial condition are:

$$\frac{\partial^2\theta}{\partial X^2} + \frac{\partial^2\theta}{\partial Y^2} = U(X,Y)\frac{\partial\theta}{\partial Z}, \tag{17}$$

$$\left.\frac{\partial\theta}{\partial X}\right|_{X=0} = 0, \tag{18}$$

$$\left[\theta + \beta(\beta_v Kn)\frac{\partial\theta}{\partial X}\right]_{X=\hat{a}} = 0, \tag{19}$$

$$\left.\frac{\partial\theta}{\partial Y}\right|_{Y=0} = 0, \tag{20}$$

$$\left[\theta + \beta(\beta_v Kn)\frac{\partial\theta}{\partial Y}\right]_{Y=\hat{b}} = 0, \tag{21}$$

$$\theta|_{Z=0} = 1. \tag{22}$$

The solution to the problem given by Eqs. (17)–(22) cannot be acquired using classical methods, such as separation of variables and the classical integral transform technique, since the velocity solution and the related eigenvalue problem are non-separable. Aparecido and Cotta [17] and Cotta [18] used a modified generalized integral transform technique to solve the problem of thermally developing laminar flow in a rectangular duct. The authors claimed that the method is computationally inexpensive and efficient. This method will also be used here as it provides the means to overcome the non-separable nature of the problem. First, two auxiliary problems are created that alleviate the difficulties associated with the eigenvalue problem. The first auxiliary problem is:

$$\frac{d^2\psi(\eta,X)}{dX^2} + \eta^2\psi(\eta,X) = 0, \tag{23}$$

$$\left.\frac{d\psi(\eta,X)}{dX}\right|_{X=0} = 0, \tag{24}$$

$$\left[\psi(\eta,X) + \beta(\beta_v Kn)\frac{d\psi(\eta,X)}{dX}\right]_{X=\hat{a}} = 0. \tag{25}$$

The second auxiliary problem is

$$\frac{d^2\omega(\xi,Y)}{dY^2} + \xi^2\omega(\xi,Y) = 0, \tag{26}$$

$$\left.\frac{d\omega(\xi,Y)}{dY}\right|_{Y=0} = 0, \tag{27}$$

$$\left[\omega(\xi,Y) + \beta(\beta_v Kn)\frac{d\omega(\xi,Y)}{dY}\right]_{Y=\hat{b}} = 0. \tag{28}$$

The eigenfunctions from the two auxiliary problems are $\psi_i = \cos(\eta_i X)$ and $\omega_m = \cos(\xi_m Y)$, respectively, while the corresponding eigenvalues can be determined from the following two transcendental equations:

$$\cot(\eta_i\hat{a}) = \beta(\beta_v Kn)\eta_i, \quad i = 1,2,3,\ldots, \tag{29}$$

$$\cot(\xi_m\hat{b}) = \beta(\beta_v Kn)\xi_m, \quad m = 1,2,3,\ldots \tag{30}$$

The auxiliary problems allow the creation of an integral transform pair that utilize the eigenfunctions and eigenvalues defined immediately above. This integral transform pair is:

Transform

$$\bar{\theta}^*_{im}(Z) = \int_0^{\hat{a}}\int_0^{\hat{b}} \cos(\eta_i X)\cos(\xi_m Y)\theta(X,Y,Z)\,dX\,dY. \tag{31}$$

Inversion

$$\theta(X,Y,Z)=\sum_{i=1}^{\infty}\sum_{m=1}^{\infty}(M_iM_m)^{-1}\cos(\eta_iX)\cos(\xi_mY)\bar{\theta}^*_{im}(Z), \tag{32}$$

where

$$M_i=\frac{\hat{a}}{2}+\frac{\sin(2\eta_i\hat{a})}{4\eta_i},\quad M_m=\frac{\hat{b}}{2}+\frac{\sin(2\xi_m\hat{b})}{4\xi_m}. \tag{33}$$

Eq. (17) is now operated on by

$$\int_0^{\hat{a}}\int_0^{\hat{b}}\cos(\eta_iX)\cos(\xi_mY)\,\mathrm{d}X\,\mathrm{d}Y. \tag{34}$$

After applying the inversion formula given by Eq. (32) and applying orthogonal properties of the eigenfunctions, this procedure will yield

$$\sum_{j=1}^{\infty}\sum_{n=1}^{\infty}D_{ijmn}\frac{\mathrm{d}\bar{\theta}^*_{jn}(Z)}{\mathrm{d}Z}+(\eta_i^2+\xi_m^2)\bar{\theta}^*_{im}(Z)=0, \tag{35}$$

where

$$D_{ijmn}=\frac{1}{M_jM_n}\int_0^{\hat{a}}\int_0^{\hat{b}}\cos(\eta_iX)\cos(\eta_jX)\cos(\xi_mY)\times\cos(\xi_nY)U(X,Y)\,\mathrm{d}X\,\mathrm{d}Y. \tag{36}$$

The transformed initial condition becomes

$$\bar{\theta}^*_{im}(0)=(\eta_i\xi_m)^{-1}\sin(\eta_i\hat{a})\sin(\xi_m\hat{b}). \tag{37}$$

The double integral in Eq. (36) can be evaluated to produce

$$D_{ijmn}=\frac{A}{M_jM_n}\sum_{k=1}^{\infty}B_k\Phi_{ijk}\Phi^*_{mnk}, \tag{38}$$

where

$$\Phi_{ijk}=\Phi_c-\left[2(1+(\beta_vKn)\phi_k\tanh(\phi_k\hat{a}))\right]^{-1}\times\left[\frac{(\eta_i+\eta_j)\sin\left[(\eta_i+\eta_j)\hat{a}\right]+\phi_k\cos\left[(\eta_i+\eta_j)\hat{a}\right]\tanh(\phi_k\hat{a})}{(\eta_i+\eta_j)^2+\phi_k^2}+\frac{(\eta_i-\eta_j)\sin\left[(\eta_i-\eta_j)\hat{a}\right]+\phi_k\cos\left[(\eta_i-\eta_j)\hat{a}\right]\tanh(\phi_k\hat{a})}{(\eta_i-\eta_j)^2+\phi_k^2}\right], \tag{39}$$

$$\Phi_c=\begin{cases}0 & \text{when } \eta_i\neq\eta_j,\\ \frac{1}{2}\left[\hat{a}+\{\sin[(\eta_i+\eta_j)\hat{a}]/(\eta_i+\eta_j)\}\right] & \text{when } \eta_i=\eta_j,\end{cases} \tag{40}$$

$$\Phi^*_{mnk}=\frac{1}{4}\left[\frac{\sin\left[(\xi_m+\xi_n+\phi_k)\hat{b}\right]}{\xi_m+\xi_n+\phi_k}+\frac{\sin\left[(\xi_m+\xi_n-\phi_k)\hat{b}\right]}{\xi_m+\xi_n-\phi_k}+\frac{\sin\left[(\xi_m-\xi_n+\phi_k)\hat{b}\right]}{\xi_m-\xi_n+\phi_k}+\frac{\sin\left[(\xi_m-\xi_n-\phi_k)\hat{b}\right]}{\xi_m-\xi_n-\phi_k}\right]. \tag{41}$$

Eqs. (35)–(41) together produce a infinite system of coupled first-order ordinary differential equations with constant coefficients that can be solved for the transformed potentials $\bar{\theta}^*_{im}$. This infinite system, however, must be truncated to a sufficiently large finite order such that the desired accuracy is produced. The truncated system of equations is written as:

$$\sum_{j=1}^{N}\sum_{n=1}^{N^*}D_{ijmn}\frac{\mathrm{d}\bar{\theta}^*_{jn}(Z)}{\mathrm{d}Z}+(\eta_i^2+\xi_m^2)\bar{\theta}^*_{im}(Z)=0,\quad i=1,2,\ldots,N,\quad m=1,2,\ldots,N^*. \tag{42}$$

The finite system can be expressed in matrix form and solved using well-known algorithms readily available in commercial software packages. Once the transformed potentials are found, the inversion formula given by Eq. (32) is invoked to compute the complete temperature profile

$$\theta(X,Y,Z)=\sum_{i=1}^{N}\sum_{m=1}^{N^*}(M_iM_m)^{-1}\cos(\eta_iX)\times\cos(\xi_mY)\bar{\theta}^*_{im}(Z). \tag{43}$$

The non-dimensional mixed mean fluid temperature can then be determined from its definition

$$\theta_m(Z)=\frac{1}{A_c}\int_{A_c}U(X,Y)\theta(X,Y,Z)\,\mathrm{d}A_c=\frac{A}{2\hat{a}\hat{b}}\sum_{k=1}^{N}\sum_{i=1}^{N}\sum_{m=1}^{N^*}(M_iM_m)^{-1}B_kQ_{km}P_{ki}\bar{\theta}^*_{im}(Z), \tag{44}$$

where

$$Q_{km}=\begin{cases}\hat{b}+\sin\left[(\phi_k+\xi_m)\hat{b}\right]\times(\phi_k+\xi_m)^{-1} & \text{when } \phi_k=\xi_m,\\ [(\phi_k-\xi_m)\sin[(\phi_k+\xi_m)\hat{b}]+(\phi_k+\xi_m)\sin[(\phi_k-\xi_m)\hat{b}]]\times(\phi_k^2-\xi_m^2)^{-1} & \text{when } \phi_k\neq\xi_m,\end{cases} \tag{45}$$

$$P_{ki}=\frac{\sin(\eta_i\hat{a})}{\eta_i}-\frac{\eta_i\sin(\eta_i\hat{a})+\phi_k\cos(\eta_i\hat{a})\tanh(\phi_k\hat{a})}{(\eta_i^2+\phi_k^2)\left[1+(\beta_vKn)\phi_k\tanh(\phi_k\hat{a})\right]}. \tag{46}$$

The local Nusselt number $Nu(Z)$ can be determined from an energy balance on a fluid element, which utilizes the axial gradient of the mixed mean temperature, to produce

$$Nu(Z) = \frac{h(z)D}{k} = -\frac{1}{4\theta_m(Z)}\frac{\mathrm{d}\theta_m(Z)}{\mathrm{d}Z}. \quad (47)$$

The mean Nusselt number can then be computed from

$$Nu_{\mathrm{m}}(Z) = \frac{1}{Z}\int_0^z Nu(Z')\mathrm{d}Z' = -\frac{1}{4Z}\ln[\theta_m(Z)]. \quad (48)$$

It can be shown that the non-slip-flow solutions derived by Aparecido and Cotta [17] are readily recovered from the above solution by setting $\beta_{\mathrm{v}}Kn = 0$.

3. Results and discussion

Numerical results for the solution of the set of initial value problems for the first-order ordinary differential equation system were obtained through the use of the matrix operations in MATLAB. A sensitivity analysis was performed to determine the optimum finite number of terms to include in the infinite series contained in the analytical solution. Values of $N = N^* = 20$ were determined to provide the desired level of convergence and accuracy for $Z > 10^{-4}$ (consistent with Aparecido and Cotta [17]). Values less than 20 resulted in poor convergence or accuracy while values greater than 20 increased the computational time (found to vary with N^5) significantly without an improvement in accuracy.

The solution method was validated by comparing results obtained for the fully developed Nusselt number for non-slip-flow $Nu_{\infty,\mathrm{ns}}$ with similar data available in the literature (Table 1). Considering the fact that data from the literature was obtained from reported correlations, good agreement was obtained between the current solutions and those from the literature for a wide range of aspect ratio. A fully developed thermal condition was assured by setting $Z = 30$ in the determination of $Nu_{\infty,\mathrm{ns}}$ from Eq. (47). With the location far downstream from the microchannel entrance, convergence may be obtained with acceptable accuracy with low values of N and N^*. Therefore, $N = N^* = 5$ were used for computational efficiency to obtain the $Nu_{\infty,\mathrm{ns}}$ data.

A dimensional analysis and the solution given by Eqs. (11)–(16) indicate that the velocity U is a function of X, Y, R, and $\beta_{\mathrm{v}}Kn$. Considering that temperature θ is a function of U and the problem statement given by Eqs. (17)–(22), θ, θ_m, and Nu are all functions of X, Y, Z, R, β, and $\beta_{\mathrm{v}}Kn$. The product $\beta_{\mathrm{v}}Kn$ provides a measure of the rarefaction that results in slip-flow, while β indicates properties of the fluid/wall interaction. Setting $\beta_{\mathrm{v}}Kn = 0$ produces a particular case in which both velocity slip and temperature jump are absent, recovering the classical case. $\beta_{\mathrm{v}}Kn$ typically has a range from 10^{-3} to 10^{-1}, corresponding to the slip-flow region. On the other hand, β influences the temperature profile alone. Thus, $\beta = 0$ artificially removes temperature jump while maintaining velocity slip. It should be noted that $\beta = 0$ implies that $F_{\mathrm{t}} = 2$, which is not physically possible. However, $\beta = 0$ provides the comparative base case for the effects of the temperature jump boundary condition. Referring to the values of F_{t} and F_{v} given in [1,15], β may be in a wide range from close to unity to more than 100 for actual wall surface conditions. β is assumed to vary in the range from 0 to 10 for the studies presented here. It should also be noted that $\beta \approx 1.667$ is a typical value for many engineering applications, corresponding to $F_{\mathrm{v}} = 1, F_{\mathrm{t}} = 1$, $\gamma = 1.4$, and $Pr = 0.7$.

The developing mixed mean temperature over the full slip-flow regime is illustrated in Fig. 1 for a nominal aspect ratio of $R = 2$ and $\beta = 1.667$. The rarefaction effect is shown to produce an increase in the local mixed mean temperature θ_{m} for increasing slip-flow. Increasing rarefaction effects also increase the thermal entrance length, although fully developed conditions are obtained at approximately $Z = 0.7$ for all $\beta_{\mathrm{v}}Kn$. The effect of β on the developing mixed mean temperature are similar, as shown in Fig. 2 for $R = 2$ and $\beta_{\mathrm{v}}Kn = 0.04$.

The axial development of the local Nusselt number Nu over the entire slip-flow regime is shown in Figs. 3–5 for $R = 2$ and $\beta = 0.1, 0.5$, and 1.667, respectively. For $\beta = 0.1$, increasing $\beta_{\mathrm{v}}Kn$ increases Nu and Nu_{∞}. This trend becomes less obvious in Fig. 4 for $\beta = 0.5$. Increasing $\beta_{\mathrm{v}}Kn$ to 0.04 increases Nu over the continuum value; however, further increases in $\beta_{\mathrm{v}}Kn$ result in decreases in Nu. Increasing β to 1.667 (Fig. 5) results in a trend that is the reverse of that shown in Fig. 3. Now, increasing $\beta_{\mathrm{v}}Kn$ produces a decrease in the heat transfer when compared to the continuum condition. These heat transfer effects may be explained by considering the physical significance of the rarefaction

Table 1
$Nu_{\infty,\mathrm{ns}}$ for $\beta_{\mathrm{v}}Kn = 0$ (non-slip flow), $N = 5$, and $Z = 30$

R	1	2	3	4	5	6	8	10
Present results	2.978	3.392	3.958	4.440	4.828	5.138	5.593	5.907
Aparecido and Cotta [17]	2.978	3.392	3.958	4.440	4.810	5.143	5.607	5.930
Shah and London [20]	2.979	3.389	3.950	4.435	4.826	5.138	5.596	5.911
Miles and Shih [20]	2.976	3.391	3.956	4.439	NA	5.137	5.595	NA

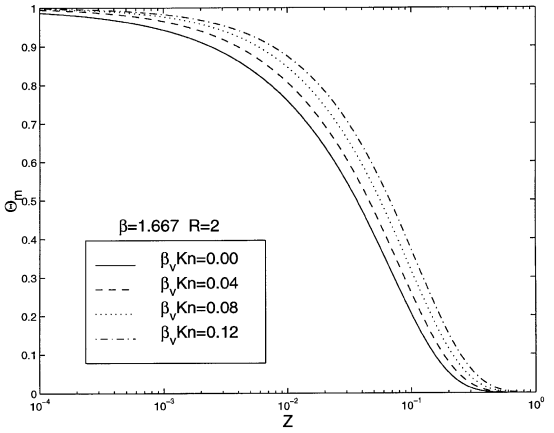

Fig. 1. Axial development of mixed mean temperature parameterized with $\beta_v Kn$ for $R = 2$ and $\beta = 1.667$.

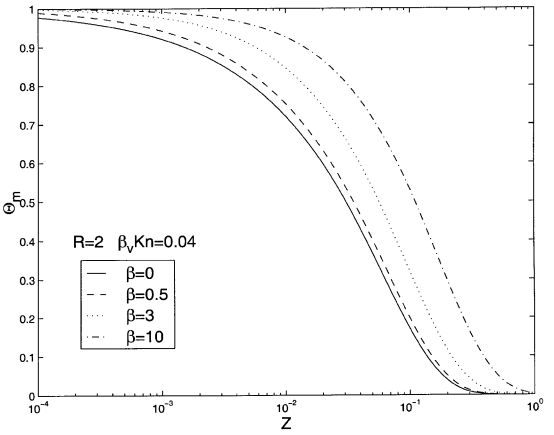

Fig. 2. Axial development of mixed mean temperature parameterized with β for $R = 2$ and $\beta_v Kn = 0.04$.

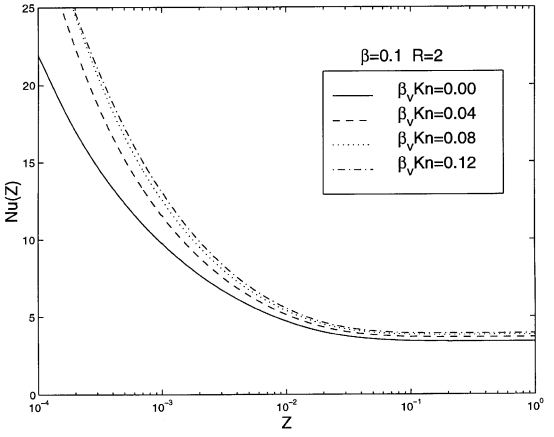

Fig. 3. Developing Nu for $R = 2$ and $\beta = 0.1$ and parameterized with $\beta_v Kn$.

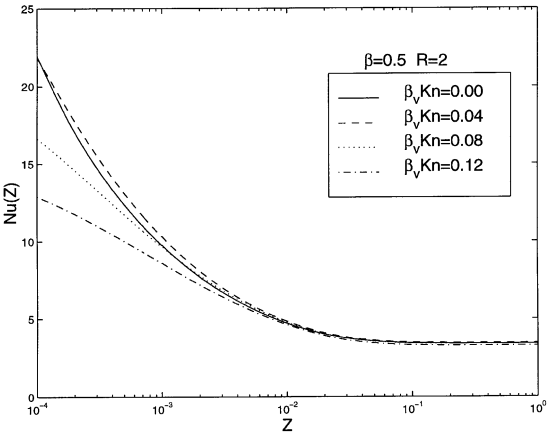

Fig. 4. Developing Nu for $R = 2$ and $\beta = 0.5$ and parameterized with $\beta_v Kn$.

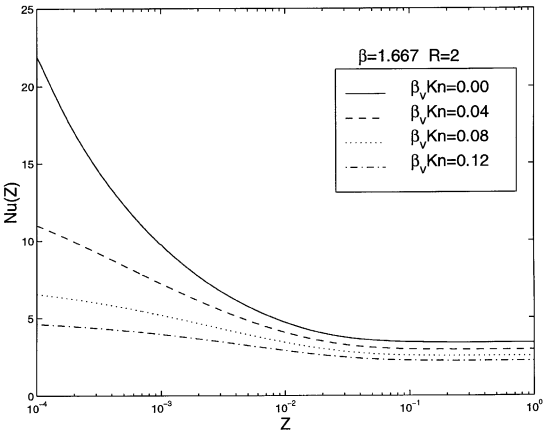

Fig. 5. Developing Nu for $R = 2$ and $\beta = 1.667$ and parameterized with $\beta_v Kn$.

effects with the departure from the continuum state. With increasing rarefaction, less momentum and energy transport will occur as velocity slip and temperature jump decrease the velocity and temperature gradients at the surfaces [1]. For low β, the increasing slip velocity that accompanies the increase in $\beta_v Kn$ dominates and heat transfer is enhanced. At large β, on the other hand, the decrease in temperature gradient at the surfaces that accompanies the increased temperature jump dominates and, thus, heat transfer decreases.

The effect of temperature jump on the axial evolution of Nu is shown in Fig. 6 for $R = 2$ and $\beta_v Kn = 0.04$ (a mid-slip-flow regime condition). Excluding temperature jump ($\beta = 0$) produces an apparent increase in heat transfer. When temperature jump is properly accounted for, increasing β results in a decrease in heat transfer. Once again, this effect is a result of the decreasing wall

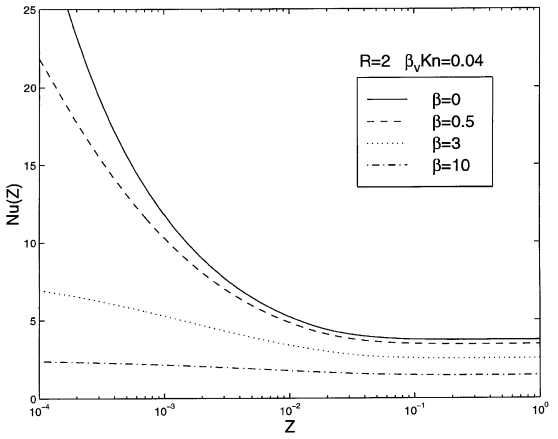

Fig. 6. Developing Nu for $R = 2$ and $\beta_v Kn = 0.04$ for a wide range of β.

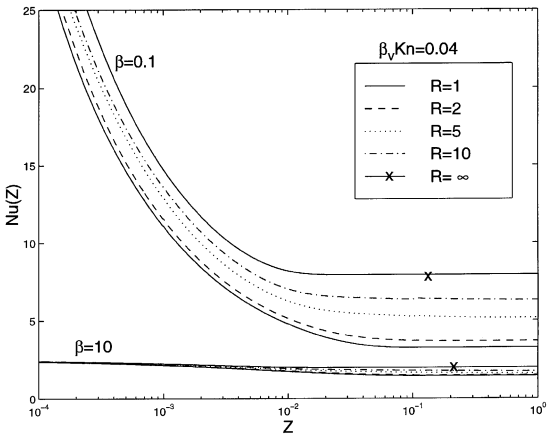

Fig. 7. Effect of aspect ratio R on developing Nu for $\beta_v Kn = 0.04$ and for both high and low β.

normal temperature gradient with β. Note that at large β, the Nu profile is nearly flat, indicating a shortened entrance length, and that considerable parametric differences in Nu are present near the microchannel entrance. In fact, $Nu(0)$ can be shown to be finite for slip-flow conditions. Yu and Ameel [19] have proposed that for either isothermal or isoflux boundary conditions in a channel of any cross-section that $Nu(0) = 1/(\beta\beta_v Kn)$.

The effect of aspect ratio on the axial development of Nu for both low and high values of β and $\beta_v Kn = 0.04$ is shown in Fig. 7. Data for $R = \infty$, originally reported by Yu and Ameel [11], is included in Figs. 7 and 8 for completeness. At low β, heat transfer increases with increasing aspect ratio, which is consistent with the non-slip solutions of Aparecido and Cotta [17]. At high β, the Nu profile is nearly flat, once again indicating a shortened entrance length. In addition,

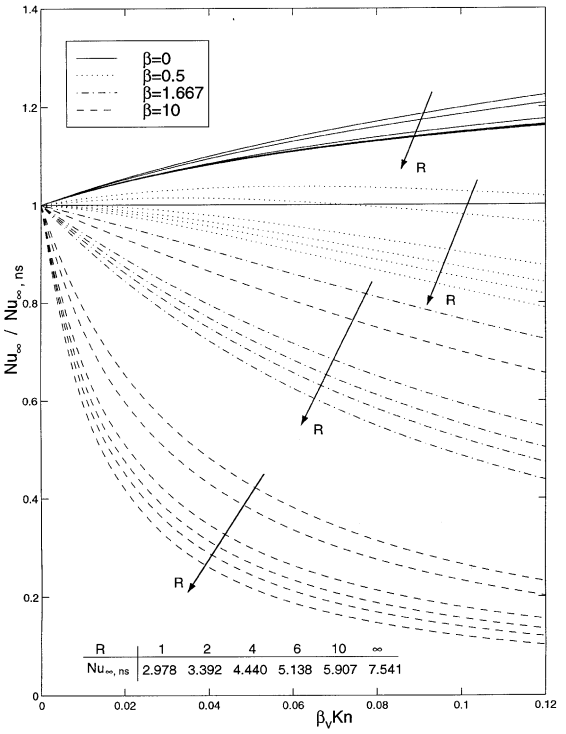

Fig. 8. Effects of R, β, and $\beta_v Kn$ on normalized Nu_∞ (normalization utilizes the corresponding non-slip Nu_∞ at the same R).

heat transfer is less than that at low β while there is little effect of aspect ratio on Nu. This indicates that temperature jump effects dominate over the effects of the channel geometry.

Heat transfer for thermally fully developed flow is of particular interest. The complete parametric analysis of Nu_∞ is presented in Fig. 8, where the Nusselt number data have been normalized with the non-slip-flow Nusselt number $Nu_{\infty,ns}$ at the same aspect ratio. Values of $Nu_{\infty,ns}$ are provided to facilitate estimates of actual values of Nu_∞ for a given combination of $\beta_v Kn$, β, and R. Normalized Nu_∞ is shown to decrease with both increasing β and increasing R, independent of $\beta_v Kn$. Note that this normalized Nu_∞ trend with respect to R is the opposite of that for Nu_∞ due to the increase in $Nu_{\infty,ns}$ with R. Heat transfer is shown to increase, decrease, or remain nearly unchanged in comparison with non-slip-flow, depending on the combination of the three independent parameters. The maximum increase and decrease in heat transfer are approximately 20% and 80%, respectively. For most engineering applications, where $\beta = 1.667$, heat transfer is always reduced when slip-flow occurs; the degree of reduction can be on the order of 40%. The data shown in Fig. 8 for $R = 1$ agree very closely with the data given by Larrode et al. [10] for a circular tube. The trends are the same and the actual

Table 2
β transition values (β_c)

R	1	2	3	4	5	6	8	10	∞
β_c	0.67	0.50	0.38	0.32	0.29	0.28	0.27	0.25	0.20[a]

[a] From Yu and Ameel [11].

values agree within the accuracy available from graphical data.

For a given aspect ratio, a transition β may be estimated that separates the region of heat transfer enhancement from that of heat transfer reduction. For instance, at $R = 2, \beta \approx 0.5$ represents this transition point. Thus, for $\beta < 0.5$, heat transfer is enhanced while for $\beta > 0.5$, heat transfer is reduced. Furthermore, heat transfer increases with increasing $\beta_v Kn$ for $\beta < 0.5$ but decreases with increasing $\beta_v Kn$ for $\beta > 0.5$. At $\beta = 0.5$, heat transfer may either increase (for $\beta_v Kn < 0.07$) or decrease (for $\beta_v Kn > 0.07$). Similar β transition values (β_c) for other aspect ratios are determined from the value of β for which the normalized Nu is unity at $\beta_v Kn \approx 0.07$. Values of β_c as a function of R are given in Table 2. Note that β_c decreases with increasing R.

4. Conclusions

The slip-flow heat transfer problem in rectangular ducts with constant wall temperature, representative of gas flow in a microchannel, has been studied. A modified generalized integral transform method has been used to solve the energy equation for the developing temperature field. This method was implemented in response to the non-separable nature of the velocity profile and corresponding eigenvalue problem. Along with the channel aspect ratio, two non-dimensional variables, $\beta_v Kn$ and β, strongly influence heat transfer. $\beta_v Kn$ represents a measure of the departure from the continuum regime (with accompanying rarefaction effects) while β is a property of the gas–surface interaction. Heat transfer was found to increase, decrease, or remain unchanged, compared to non-slip-flow conditions, subject to values of $\beta_v Kn, \beta$, and R. A transition value β_c that separates the regions of heat transfer enhancement and heat transfer reduction was determined as a function of aspect ratio. β_c was found to decrease with increasing aspect ratio. For a given aspect ratio, increasing temperature jump (or β) always reduces heat transfer. Thermal entrance length was shortened when β increases. The normalized fully developed Nusselt number was found to decrease with increasing aspect ratios. For small β, heat transfer increases with increasing aspect ratio, but for large β this effect becomes negligible. The effects of β and $\beta_v Kn$ on heat transfer are a result of the reduction of the wall normal velocity and temperature gradients with the increasing velocity and temperature jump that accompany the departure from the continuum regime.

References

[1] E.G.R. Eckert, R.M. Drake, Jr., Analysis of Heat and Mass Transfer, McGraw-Hill, New York, 1972, pp. 467–486.
[2] J.Q. Liu, Y.C. Tai, C.M. Ho, MEMS for pressure distribution studies of gaseous flows in microchannels, Proc. IEEE Micro-electromech. Syst. (1995) 209–215.
[3] E.B. Arkilic, K.S. Breuer, M.A. Schmidt, Gaseous flow in microchannels, Application of Micro-fabrication to Fluid Mechanics, ASME FED-Vol. 197, 1994, 57–66.
[4] Y.P. Shih, C.C. Huang, S.Y. Tsay, Extended Leveque solution for laminar heat transfer to power-law fluids in pipes with wall slip, Int. J. Heat Mass Transfer 38 (1995) 403–408.
[5] R.F. Barron, X.M. Wang, R.O. Warrington, T.A. Ameel, Evaluation of the eigenvalues for the Graetz problem in slip-flow, Int. Commun. Heat Transfer 23 (1996) 563–574.
[6] R.F. Barron, X.M. Wang, T.A. Ameel, R.O. Warrington, The Graetz problem extended to slip flow, Int. J. Heat Transfer 40 (1997) 1817–1823.
[7] X.M. Wang, Evaluation of the eigenvalues of the Graetz problem in slip-flow, M.S. Thesis, Louisiana Tech University, Ruston, Louisiana, 1996.
[8] T.A. Ameel, R.F. Barron, X.M. Wang, R.O. Warrington, Laminar forced convection in a circular tube with constant heat flux and slip flow, Microscale Thermophys. Eng. 1 (1997) 303–320.
[9] M.L. Wang, T.A. Ameel, A.B. Frazier, R.O. Warrington, Microtube convection heat transfer for a power-law fluid in laminar slip flow with an isoflux boundary condition, in: International Mechanical Engineering Congress and Exposition, Anaheim, CA, HTD-Vol. 361–3, November 1998, pp. 157–164.
[10] F.E. Larrode, C. Housiadas, Y. Drossinos, Slip-flow heat transfer in circular tubes, Int. J. Heat Transfer 43 (2000) 2669–2680.
[11] S.P. Yu, T.A. Ameel, Slip flow low Peclet number thermal entry problem within a flat microchannel subject to constant wall temperature, in: Proceedings of the Conference on Heat Transfer and Transport Phenomena in Microsystems, Banff, Alta., Canada, October 2000.
[12] I. Papautsky, J. Brazzle, H. Swerdlow, A.B. Frazier, A low temperature, IC compatible process for fabricating surface micromachined metallic microchannels, IEEE J. Microelectromech. Syst. 7 (1998) 267–273.
[13] R.S. Stanley, R.F. Barron, T.A. Ameel, Two-phase flow in microchannels, in: International Mechanical Engineering Congress and Exposition, Dallas, TX, November 1997.

[14] W.M. Rohsenow, J.P. Hartnett, in: Handbook of Heat Transfer, McGraw-Hill, New York, 1973, pp. 9.1–9.8.
[15] R. Goniak, G. Duffa, Corrective term in wall slip equations for Knudsen layer, J. Thermophys. 9 (1995) 383–384.
[16] W.A. Ebert, E.M. Sparrow, Slip flow in rectangular and annular ducts, Trans. ASME (1965) 1018–1024.
[17] J.B. Aparecido, R.M. Cotta, Thermally developing laminar flow inside rectangular ducts, Int. J. Heat Transfer 33 (1990) 341–347.
[18] R.M. Cotta, in: Integral Transforms in Computational Heat and Fluid Flow, CRC Press, Boca Raton, Florida, 1993, pp. 180–188.
[19] S.P. Yu, T.A. Ameel, A universal entrance Nusselt number for internal slip flow, Int. Commun. Heat Mass Transfer, in review.
[20] R.K. Shah, A.L. London, Laminar flow forced convection in ducts, Adv. Heat Transfer Suppl. (1978) 196–222.